Structures of Steps and Appearances of {311} Facets on Si(100) Surfaces

Atsushi Oshiyama

Fundamental Research Laboratories, NEC Corporation, Miyukigaoka, Tsukuba 305, Japan

(Received 14 July 1994)

First-principles total-energy calculations for structures and reactivities of single-, double-, and quadrilayer steps on Si(100) surfaces are presented. It is found that an activation energy for diffusion of an adatom on an upper terrace increases near a step edge and that rebonded and nonrebonded steps show bistability. A new reaction pathway in which the rebonded double-layer steps bunch and lead to a {311} facet is found to be energetically favorable.

PACS numbers: 68.35.Bs, 68.35.Md, 68.55.Jk, 82.65.Dp

Unexpected appearances of small areas of high-Miller-index surfaces (facets) on lower-Miller-index substrate surfaces are well known phenomena in nature. An example commonly observed is the appearance of the {311} facet of Si: It was observed during homoepitaxial and heteroepitaxial growth on Si(100) substrates [1,2], or by annealing thin {110}-oriented Si specimens in vacuum [3]. One may interpret these observations of {311} faceting as the (311) surface having low surface energy. Recent first-principles calculations, however, have shown that the (311) surface has higher energy than its low-Miller-index counterparts [4]. A notion that the (311) surface is *not* thermodynamically stabler than the (100) surface has also been corroborated by examination of void shapes in Si [5]. Carbon contamination is then speculated as a possible origin of the {311} faceting [1,4]. Recently, Hirayama, Hiroi, and Ide argued that the {311} facet appears due to bunching of double-layer steps inherent to the Si(100) surface based on their electron microscope observations of Si epitaxial layers [6].

The aim of the present work is thus twofold. First, I present first-principles total-energy calculations for structures and reactivities of single- (S), double- (D), and quadri- (Q) layer steps on the Si(100) surface. The results provide a firm theoretical framework for understanding step-related atomic reactions during an initial stage of epitaxial growth. A controversy about the structure of the double-layer step among the two independent tight binding calculations [7,8] and the scanning tunneling microscopy (STM) measurement [9] is also resolved. Second, I investigate step-related kinetic pathways leading to the appearance of the {311} facet. I indeed find that bunching of a special type of double-layer steps is an energetically favorable pathway and that the resulting facet has the Miller index of (311).

We first set out classification of steps on the Si(100). Each pair of top-layer Si atoms on the (100) surface forms a dimer, and the dimer rows are aligned along the $\langle 011 \rangle$ direction. Hence there are two distinct types for each S, D, or Q step: one where the step edge is parallel to the dimer-row direction on an upper terrace and the other where it is normal, labeled by the subscripts A and B, respectively. Further, there is a possibility of forming Si pentagons at the edge to saturate the dangling bonds (rebonded structure) [8]. Whether the rebonded structure has lower energy than the nonrebonded structure is, however, subtle due to bond-length strains in the Si pentagons in the rebonded structure.

Formation energies of the steps are calculated by using repeating slab geometries in which the bottom of the slab is terminated by H atoms. Following Chadi [8], I use the (15,1,1) vicinal surface which contains one of D_A, D_B, and $S_A + S_B$ steps in a periodic cell and obtain differences in formation energies λ: i.e., $\lambda(D_A) - [\lambda(S_A) + \lambda(S_B)]$ and $\lambda(D_B) - [\lambda(S_A) + \lambda(S_B)]$. The periodicity along the step edge is taken to be double the surface lattice constant $a \simeq 3.84$ Å. I also use the (8,1,1) vicinal surface to examine stability of the Q_B step and the periodic step arrays with the 2×6 lateral periodicity to obtain individual formation energies $\lambda(S_A)$ and $\lambda(D_B)$. All calculations are carried out by the use of norm-conserving pseudopotentials [10] and the local density approximation (LDA) [11] combined with the conjugate-gradient minimization technique as reported elsewhere [12]. All calculational parameters have been examined carefully, and we find that the 8-Ry cutoff energy in the plane wave basis set, the $3 - k$ points in half the surface Brillouin zone, and more than 5 Si atomic layers and the 7.3 Å vacuum region in the slab model are necessary to obtain converged results. The geometry optimization has been performed for all atoms in the slab except for the bottom-most Si and H atoms. In the optimized geometries the remaining forces acting on the atoms are less than 0.004 Ry/Å.

For the flat Si(100), it is found that the 2×1 buckled-dimer surface is lower in energy than the symmetric-dimer surface by 0.10 eV per dimer. Alternation of the buckled dimers along the dimer row leading to $p(2 \times 2)$ periodicity further induces the energy gain of 0.13 eV per dimer. The amount of the dimer buckling is 0.72 Å in the alternating buckled-dimer geometry. These results reasonably agree with those from the previous LDA calculations [13,14]. The step formation energy presented below is defined as the total-energy cost to form the step from the alternating buckled-dimer flat surface. Continuum elastic theory pre-

 0031-9007/95/74(1)/130(4)$06.00

dicts that force dipoles along step edges lead to the step formation energy contribution varying as l^{-2} (l: terrace width) [15], and that relaxation of stress across step edges leads to the contribution varying as $\ln(l)$ [16,17]. This behavior is indeed confirmed by atomistic calculations using empirical potentials [18]. The step formation energies obtained below from the LDA calculations are thus the step energies with the particular terrace width, being an index of relative stability among the steps.

Figure 1 shows total-energy-optimized atomic structures of single- and double-layer steps. The calculated step formation energies are $\lambda(S_A) = 0.088$ eV/a for S_A, $\lambda(S_B) = 0.12$ eV/a for rebonded S_B, $\lambda(D_A) = 0.43$ eV/a for D_A, and $\lambda(D_B) = 0.17$ eV/a for rebonded D_B, respectively. The formation energies estimated from the previous tight-binding calculation using similar slab models [$\lambda(S_A) \simeq 0.01$ eV/a, $\lambda(S_B$: rebonded$) \simeq 0.15$ eV/a, $\lambda(D_A) \simeq 0.54$ eV/a, and $\lambda(D_B$: rebonded$) \simeq 0.05$ eV/a [8]] qualitatively agree with the present results. The calculated values for the monolayer steps are comparable with those estimated from the STM measurement [$\lambda(S_A) \simeq 0.028$ eV/a and $\lambda(S_B) = 0.09$ eV/a [19]] and consistent with the observation that the S_A step edge is much smoother than the S_B step edge on the Si(100). The relative energy difference, $\lambda(D_B) < \lambda(S_A) + \lambda(S_B)$, is also consistent with the observation that the D_B step appears dominantly rather than the S_A plus S_B steps on the vicinal surface, though step-step interactions as a function of l should be considered for detailed analysis [17,18].

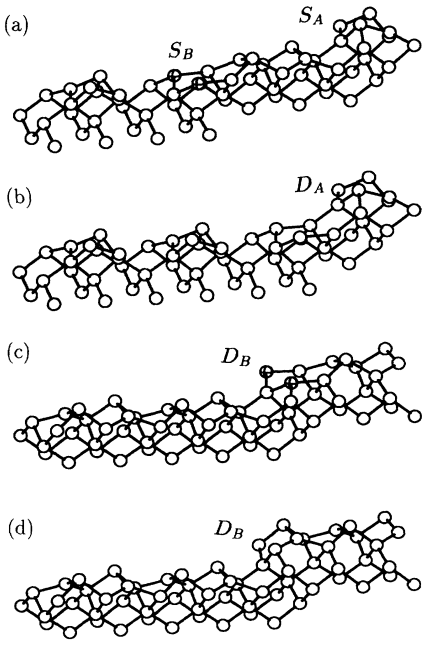

FIG. 1. Total-energy optimized atomic structures of (a) S_A plus S_B, (b) D_A, (c) rebonded D_B, and (d) nonrebonded D_B steps. Rebonded atoms are marked by crossed spheres.

For comparison of formation energies between rebonded and nonrebonded structures, chemical potential of Si atoms μ_{Si} is introduced since the number of Si atoms around the step edges are different. When we assume $\mu_{Si} = \mu_{Si(bulk)}$, we obtain $\lambda(D_B$: rebonded$) - \lambda(D_B$: nonrebonded$) = -0.06$ eV/a: The rebonded structure is stable, and the nonrebonded is metastable for the D_B step (bistability) when Si atoms are provided from the crystal reservoir.

Rebonded and nonrebonded structures show characteristic reconstructions near the step edges. In the rebonded D_B step (Fig. 1), each Si atom at the mid terrace (rebonded atom) saturates three dangling bonds and thereby gains the electronic energy in spite of the induced bond-length strains: The bond length between the rebonded atom and the upper-terrace atom is elongated by 4.7%–6.6% compared with the bulk bond length. The adjacent rebonded atoms at the mid-terrace exhibit upward and downward shifts, respectively (vertical separation of 0.17 Å), so that the stress is partially released. The amount of the buckling of the dimers becomes small (~20% reduction) near the step edges: 0.55 Å at the upper-terrace edge and 0.61 Å at the lower-terrace edge. The reduction of the buckling near the step edges is also found in the recent calculation for monolayer steps [14]. Variation of the height of the topmost Si atoms across the step edge in the optimized rebonded D_B, together with the obtained periodicity of $2a$ along the step edge, is consistent with the STM observation of the D_B step [9]. In the nonrebonded D_B step (Fig. 1) that I find is also stable, distances between the top-layer Si and the second-layer Si atoms at the step edge is 2.22 and 2.23 Å, significantly shorter than the bond length in the bulk (2.35 Å). This means that the π-bonded reconstruction takes place at the edge of the nonrebonded D_B step [20].

Which structure, the rebonded or the nonrebonded structure, is dominantly observed depends on the Si chemical potential as is stated above. It also depends on kinetic pathways in formation of the steps. In the regime of step-flow growth, the S_A step formed first is followed by the next-layer S_B step and then becomes the rebonded D_B step. The present calculation shows that the reaction is exothermic with the energy gain of 0.04 eV/a. Once the rebonded D_B step is formed, conversion from the rebonded to the nonrebonded is hindered by significant energy barriers as is shown below. We prepare the optimized rebonded D_B step [Fig. 1(c)], add an Si atom on the upper terrace, and then search most probable reaction pathways in which the Si adatom approaches the step edge and converts the rebonded geometry to the nonrebonded one [Fig. 1(d)]. This is expected to typify atomic reactions in the regime of the step-flow growth. Figure 2 shows the calculated total energy variations along the two probable reaction pathways. To obtain the reaction pathways, I place a Si adatom on the upper terrace at the fixed distance from the step edge (x in

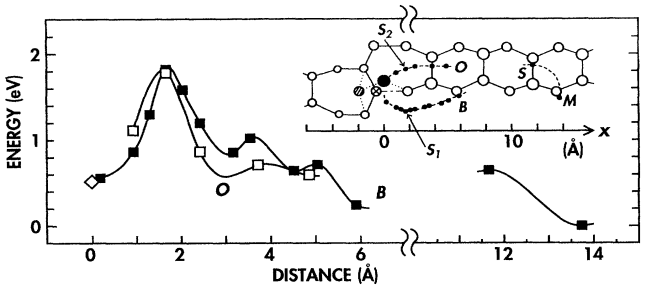

FIG. 2. Calculated total-energy variation along the reaction pathways for the conversion of the rebonded D_B step to the nonrebonded step. The inset shows a top view of the rebonded step. In the reaction, a Si adatom follows the pathway B or O (dots in the inset), cuts the bond (dash-dotted line) at the edge, and sits at the top-layer site (solid circle) with the rebonded atom (crossed circle) displaced to the lower terrace (hatched circle). The total-energy variations as a function of the distance (x) from the step edge on the upper terrace along the pathways B and O are shown by solid and open squares, respectively. The total energies on the terrace (sites S and M) and of the product nonrebonded geometry are also shown by solid squares and an open rhombus, respectively.

Fig. 2), relax all the atoms including y (parallel direction to the edge) and z (vertical direction to the surface) coordinates of the adatom, and repeat the calculations for several values of the distance x. I find the two pathways, one between the dimer rows (B) and the other on the dimer row (O), toward the nonrebonded structure.

When the adatom is located far enough (more than 10 Å) from the step edge, the total-energy variation is similar to that for the flat surface: I find that the most stable position for the adatom is the site off the dimer rows (site M in Fig. 2) and that the saddle point is the site on the dimer (site S). The calculated activation energy for diffusion along this path is 0.65 eV which reasonably agrees with the previous LDA calculation performed for the flat Si(100) surface [21].

When the adatom approaches the step edge, a further energy barrier emerges along both pathways B and O. The total energy increases as the Si adatom passes the top-layer dimer at the edge. The saddle points are the positions near the second-layer Si atom (sites S_1 and S_2 in Fig. 2). The calculated additional activation energy is 1.1 eV for both pathways. The saddle point S_1 near the second-layer Si atom corresponds to the stable binding position M on the terrace. The large binding energy at the M site is understood in terms of the adatom making three bonds with two top-layer Si atoms and one second-layer Si atom: The bond lengths are 2.36, 2.42, and 2.39 Å, respectively. At the step edge, however, one of the two top-layer Si atoms is missing. The adatom is thus located around the middle of the valley between the two dimer rows forming two bonds with the neighboring second-layer atoms: The bond lengths at the site S_1 are 2.26 and 2.56 Å. Also at the saddle point S_2 the adatom makes

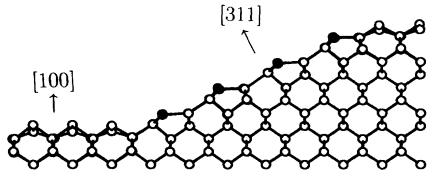

FIG. 3. View of the bunched rebonded D_B steps on Si(100) seen from the [011] direction. The rebonded atoms are denoted by solid circles.

two bonds with the lengths of 2.43 and 2.55 Å. This decrease in the number of bonds caused by missing top-layer atoms at the step edge is the origin of the additional activation energies. The present total-energy calculations clearly show that the Si adatom diffusing on the upper-terrace encounters an additional energy barrier near the step edge. This means low reactivity of the rebonded D_B step in the regime of the step-flow growth.

An increase in the activation energy for the adatom diffusion on the upper terrace is generally expected in the vicinity of any type of the step edges (the reason for the increase is the missing top-layer atoms). This indicates that the bunching of steps takes place once the flow of the step is pinned at some sites [22]. In step-flow growth on Si(100), the rebonded D_B step is formed at first, and the bunching of the D_B steps is highly expected. Figure 3 is a side view of the atomic structure caused by such bunching. The resulting facet has indeed the Miller index of (311). I have actually optimized the atomic geometry caused by the bunching of the two rebonded D_B steps (namely, the Q_B step) and found that the structure is stable [Fig. 4(a)] [23]. I thus argue that the bunching of the D_B steps is the microscopic mechanism of the appearance of the {311} facet. The new finding that validates this argument is the increase in the activation energy for the adatom diffusion near the step edge and the resulting low reactivity of the D_B step [24].

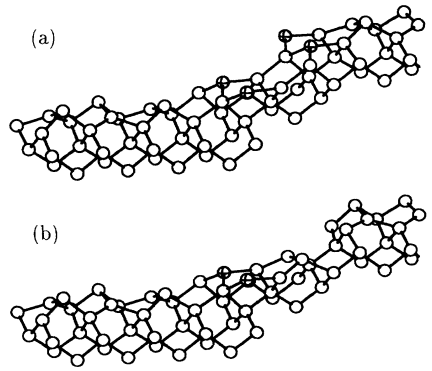

FIG. 4. Optimized geometry upon bunching of two D_B steps. (a) The bunching of the two rebonded steps, and (b) the piled nonrebonded step on the rebonded step.

The strain inherent in the rebonded structures brings additional complexity related to reconstructions of the (311) surface. I find that the rebonded Q_B step [Fig. 4(a)] is higher in energy by 0.18 eV/a than the other Q_B step [Fig. 4(b)] in which the second-layer rebonded atoms are missing. The bond stretching (~5%) in the rebonded structure causes the strain energy. The bunching of the two rebonded D_B steps is thus surpassed by the nonrebonded step on the rebonded step in which the upper nonrebonded step releases the strain energy. In fact, a half of the bonds near the step edges are elongated by 6%–9% in the optimized geometry of the two rebonded steps [Fig. 4(a)], whereas only two bonds are elongated by ~5% in the nonrebonded plus the rebonded steps [Fig. 4(b)]. The facet formed by the alternating bunching of the rebonded D_B step and the nonrebonded D_B step still has the Miller index of (311). This alternation is an example of the competition between saturating dangling bonds and releasing strain energies commonly observed in reconstructions of semiconductor surfaces; e.g., the Si(311) surface indeed shows 3×2 reconstruction in which several bonds are stretched or compressed with some atoms having dangling bonds [4,25]. Yet, the present structure obtained from the alternating bunching of the rebonded and the nonrebonded D_B steps is different from the 3×2 reconstructed structure. I speculate that there is a transition from the present structure peculiar to the small (311) surface formed by the kinetic pathway to another structure commonly observed, as the area of the facet increases.

I have shown that the D_B step formed by the reaction $S_A + S_B \rightarrow D_B$ has the rebonded structure. One may consider a different situation, however. For instance, when the Si concentration in vapor phases in epitaxial growth is high, a different reaction pathway in which the Si is adsorbed directly at step edges is open. In this case, the reaction D_B(rebonded) + Si(vapor) $\rightarrow$ D_B(nonrebonded) becomes exothermic since the chemical potential of Si in the vapor phase is higher than that in the bulk. When the bunching of the nonrebonded D_B steps takes place, the resulting facet has the Miller index of (111). This {111} facet is indeed observed in the molecular beam epitaxy with high flow rate of disilane gas source [6]. The bistability between the rebonded and the nonrebonded structures that I have found is controlled by external parameters, the vapor pressure in this case, and leads to macroscopic differences in surface morphology.

[1] Y-N. Yang and E. D. Williams, J. Vac. Sci. Technol. A **8**, 2481 (1990).

[2] N. Ohsima *et al.,* Appl. Surf. Sci. **48/49**, 69 (1991); D. J. Eaglesham, F. C. Unterwald, and D. C. Jacobson, Phys. Rev. Lett. **70**, 966 (1993).

[3] J. M. Gibson, M. L. McDonald, and F. C. Unterwald, Phys. Rev. Lett. **55**, 1765 (1985).

[4] D. M. Bird *et al.,* Phys. Rev. Lett. **69**, 3785 (1992); J. Dąbrowski *et al., ibid.,* **73**, 1660 (1994).

[5] D. J. Eaglesham *et al.,* Phys. Rev. Lett. **70**, 1643 (1993).

[6] H. Hirayama, M. Hiroi, and T. Ide, Phys. Rev. B **48**, 17 331 (1993).

[7] D. E. Aspnes and J. Ihm, Phys. Rev. Lett. **57**, 3054 (1986).

[8] D. J. Chadi, Phys. Rev. Lett. **59**, 1691 (1987).

[9] P. E. Wierenga, J. A. Kubby, and J. E. Griffith, Phys. Rev. Lett. **59**, 2169 (1987).

[10] N. Troullier and J. L. Martins, Phys. Rev. B **43**, 1993 (1991).

[11] D. M. Ceperley and B. J. Alder, Phys. Rev. Lett. **45**, 566 (1980).

[12] O. Sugino and A. Oshiyama, Phys. Rev. Lett. **68**, 1858 (1992); B. D. Yu and A. Oshiyama, Phys. Rev. Lett. **71**, 585 (1993).

[13] N. Roberts and R. J. Needds, Surf. Sci. **236**, 112 (1990); J. Dabrowski and M. Scheffler, Appl. Surf. Sci. **56-58**, 15 (1992); J. E. Northrup, Phys. Rev. B **47**, 10 032 (1993).

[14] P. Boguslawski *et al.,* Phys. Rev. Lett. **72**, 3694 (1994).

[15] V. I. Marchenko and A. Y. Parshin, Zh. Eksp. Teor. Fiz. **79**, 2576 (1980) [JETP **52**, 129 (1980)].

[16] V. I. Marchenko, Pis'ma Zh. Eksp. Teor. Fiz. **33**, 397 (1981) [JETP Lett. **33**, 381 (1980)].

[17] O. Alerhand *et al.,* Phys. Rev. Lett. **61**, 1973 (1988); **64**, 2406 (1990).

[18] T. W. Poon *et al.,* Phys. Rev. B **45**, 3521 (1992).

[19] D. S. Swartzentruber *et al.,* Phys. Rev. Lett. **65**, 1913 (1990).

[20] The π-bonded reconstruction that I find is different from that proposed in Ref. [7].

[21] G. Brocks, P. J. Kelly, and R. Car, Phys. Rev. Lett. **66**, 1729 (1991); Surf. Sci. **269/270**, 860 (1992).

[22] The pinning site is a side wall formed in the device fabrication in some epitaxial growth experiments [6] and may be defects or impurities in the case of the spontaneous appearance of the facets.

[23] Calculations for the Q_B steps are carried out using the (8,1,1) vicinal surface.

[24] The appearance of the {311} facet in the annealing experiments may also be related to the increase in diffusion barrier near step edges which constitute a macroscopic shape of the island.

[25] W. Ranke, Phys. Rev. B **41**, 5243 (1990); J. Knall *et al.,* Phys. Rev. Lett. **66**, 1733 (1991).